ChemPhysChem

Chemistry Europe
European Chemical Societies Publishing

Accepted Article

Title: Using a Nitrophenol Cocktail Screen to Improve Catalyst Down-selection

Authors: Titel Jurca, Lorianne R. Shultz, Lin Hu, and Xiaofeng Feng

To be cited as: *ChemPhysChem* 10.1002/cphc.202000400

Link to VoR: https://doi.org/10.1002/cphc.202000400

WILEY-VCH

Using a Nitrophenol Cocktail Screen to Improve Catalyst Down-selection

Lorianne R. Shultz,[a],[b] Lin Hu,[b],[c] Xiaofeng Feng,[b],[d] and Titel Jurca*[a],[b],[e]

[a] L. R. Shultz, Prof. T. Jurca
Department of Chemistry
University of Central Florida
Orlando, Florida, 32816 (USA)
E-mail: Titel.Jurca@ucf.edu
[b] L. R. Shultz, L. Hu, Prof. X. Feng, Prof. T. Jurca
Renewable Energy and Chemical Transformations Cluster
University of Central Florida
Orlando, Florida, 32816 (USA)
[c] L. Hu,
Department of Materials Science and Engineering
University of Central Florida
Orlando, Florida, 32816 (USA)
[d] Prof. X. Feng
Department of Physics
University of Central Florida
Orlando, Florida, 32816 (USA)
[e] Prof. T. Jurca
NanoScience Technology Center
University of Central Florida
Orlando, Florida, 32826 (USA)

Supporting information for this article is given via a link at the end of the document.

Abstract: The catalytic reduction of 4-nitrophenol (**4NP**) with excess $NaBH_4$ is the benchmark model for quantifying catalytic activity of nanoparticles. Although broadly useful, the reaction can be very selective. This can lead to false positives and negatives when utilized for catalyst down-selection from a broader materials candidate pool. We report a multi-nitrophenol cocktail screening methodology incorporating **4NP** and other amino-nitrophenols, utilizing Ag, Au, Pt, and Pd nanoparticles supported on carbon support. The reduction of the cocktail proceeds with no deleterious side reactions on the time-scale tested. The resulting kinetic rates provide an improved correlation of relative catalyst activity when compared to performance with other reducible moieties (e.g. azo bonds), or when compared to solely **4NP** screening.

Para-, or 4-nitrophenol (**4NP**), and more broadly, compounds in the nitroaromatic family are widely used in the fabrication of pharmaceuticals, explosives, pesticides, pigments and dyes.[1] As a result, they have become a very common anthropogenic pollutant in aqueous industrial effluent. While many nitroaromatics display acute toxicity, are mutagenic and either potential or established carcinogens,[2] their reduction products, aniline-derivatives, are typically less toxic, commercially important synthetic intermediates. For example, the reduction product of **4NP** is 4-aminophenol (**4AP**), a useful component for the synthesis of dyes, agrochemicals, and pharmaceuticals.[3] Concomitantly, due to its simplicity and reliability, the **4NP** → **4AP** reduction process has also become one of the most widely used probe reaction systems for heterogeneous catalyst development.[4-12]

When conducted in water with significant excess of $NaBH_4$ as the H-source, the reaction is commonly described in terms of the Langmuir-Hinshelwood model as a pseudo-first order process.[7] The system entails the delivery of H to the catalyst surface via $NaBH_4$ hydrolysis, which also produces H_2 that can be activated by certain catalysts at an appropriate pH.[13] Subsequent adsorption and reaction of 4-nitrophenolate (**4NP***), the resulting product of **4NP** and $NaBH_4$, with the surface leads to the hydrogenated product 4-aminophenolate (**4AP***). Its broad application is due to the ease and accuracy of extracting kinetic data via UV-Vis spectroscopic monitoring of the λ_{max} = 400 nm peak of **4NP***. Catalyst performance is quantified in terms of the apparent rate constant k_{app} (eq. 1), derived from the slope of $\ln(C/C_0)$ as a function of time; C/C_0 is obtained from the absorbance for **4NP*** at λ_{max} = 400 nm (A/A_0), collected after an induction period. This operates under the assumption that the adsorption of **4NP*** onto the catalyst surface is the rate limiting step.[7]

$$-k_{app}t = \ln\left(\frac{A}{A_0}\right) = \ln\left(\frac{C}{C_0}\right) \quad (1)$$

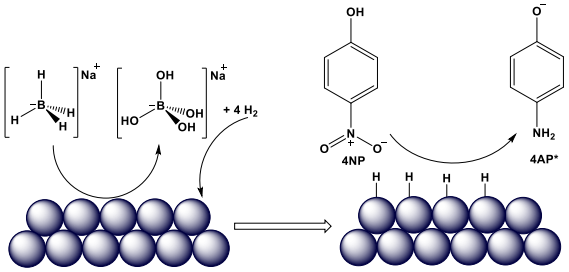

Scheme 1. General scheme for **4NP** reduction with excess $NaBH_4$ in H_2O.

The near universal use of this model reaction can, *when applied properly*, provide a unifying point of comparison when designing new heterogeneous catalysts and is thus extremely valuable.[14] Another common use of the **4NP** screen is for down-selection of

heterogeneous catalysts from a larger candidate pool, typically synthesized under variably parameterized synthetic protocols. The most active material for **4NP** reduction is typically promoted to an expanded substrate scope, then subjected to further analysis; a typical process flow is illustrated in Fig. 1. From our previous studies where all catalyst candidates were promoted to an expanded substrate scope, it became evident that the **4NP** reduction does not always select the best catalyst.[15,16] It is not surprising that different catalysts, whether they have a disparate chemical constitution via similar preparative routes, or a similar constitution via different preparative routes, exhibit distinct selectivities. However, it does call into question the prognosticating ability, and suitability of the ubiquitous **4NP** reaction for catalyst down-selection. The broader utility of the **4NP** reaction is thus not being refuted.

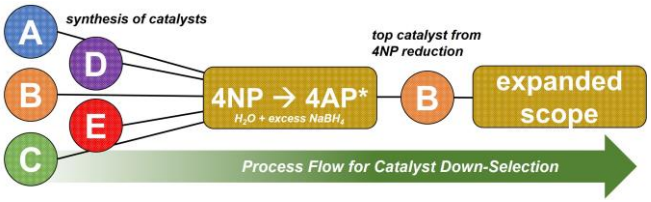

Figure 1. Illustrated flow-chart for catalyst down-selection using the **4NP → 4AP*** reaction.

In our prior report we screened a series of carbon-supported <10 nm precious metal nanoparticles; (w/w % by ICP-MS) **Au@C** (6.8 ± 0.9%), **Ag@C** (23.5 ± 0.4%), **Pt@C** (27.8 ± 1.5%), and **Pd@C** (13.5 ± 1.9%) (Fig. S1). All catalysts were first utilized for reduction of **4NP**, then a series of variably substituted aminonitrophenols (**ANPs**): 4-amino,3-nitrophenol (**4A3NP**), 2-amino,5-nitrophenol (**2A5NP**), 4-amino,2-nitrophenol (**4A2NP**). Finally, two common azo dyes methyl red (**MR**) and methyl orange (**MO**) were reduced under similar conditions, and the reduction of -NO_2 and -N=N- groups reduction was analyzed. Ultimately, we found that reaction rates varied greatly among both the nitrophenols and the azo dyes, and **4NP** offered low predictability. However, averaging weight normalized rates (K = $min^{-1}g^{-1}$; *g of metal*) across all individual nitrophenol trials led to a closer match for catalyst performance against azo groups.[15] Nonetheless, a cumbersome multi-step process is not attractive for rapid screening of multiple candidates. Herein we report the succesful application of a "cocktail" of the aforementioned **4NP** and **ANPs** which allows rapid single run screening. We compare the results to previously screened **MO** and **MR** as well as azobenzene (**AB**) and methylene blue (**MB**).[15]

To ensure a direct comparison, where possible, reactions were conducted under identical conditions to our prior report: *in-situ* (1 cm path length quartz UV cell) in 3 mL of deionized water (**DIW**), with excess $NaBH_4$. The nitrophenol cocktail was comprised of 0.39 µmol of each component; **4NP**, **4A3NP**, **2A5NP**, **4A2NP** (Scheme 2A). **AB** and **MB** screening was conducted with 0.39 µmol and 0.083 µmol of reagents respectively (Scheme 2B), with **AB** in a 2:1 H_2O:EtOH solution to aid solubility. After recording a t_0 absorbance, 1 mg of catalyst was added and stirred gently for ~2 s. The reactions were allowed to proceed without further intervention and monitored at fixed intervals by the decreasing absorbance at the defined maxima (*vide infra*). All catalysts promote hydrolysis of $NaBH_4$ to some degree[17] (Scheme 1) which leads to a turbid solution, resulting in artificially increased baseline absorbance (up to ~1 a.u.); this is most pronounced for **Pd@C** and **Pt@C**. To enable data extraction under these conditions, spectra were normalized to the baseline, and k_{app} was assigned to the initial few data points prior to significant noise from H_2 evolution. Further details are provided in the Supporting Information.

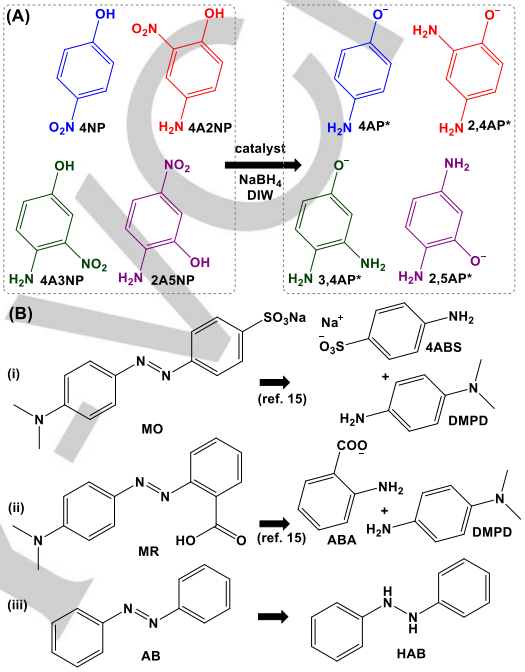

Scheme 2. Catalytic reduction of (A) nitrophenol cocktail and (B) azo dyes **MO** and **MR** and azobenzene (**AB**) by metal nanoparticles in DIW with excess $NaBH_4$. ***MO* and *MR* reduction has been previously reported in ref. 15.**

The cocktail results in a cumulative bimodal peak in the visible region with a maximum at λ_{max} = 400 nm, and a shoulder at λ = 500 nm (Fig. 2). To obtain k_{app} for the cocktail, the decrease in absorbance intensity of both the maxima (400 nm) and shoulder (500 nm) were monitored, and the values across both observed peaks were averaged (k_{avg}); this is done to ensure that rate is not biased towards the main constituents of each peak (i.e. **4NP*** and **2A5NP*** at 400 nm, and **4A2NP*** and **4A3NP*** at 500 nm) (Fig. S2). When normalized to %metal content, K_{avg} values yield 1659.6 ± 40.5 $min^{-1}g^{-1}$ (**Ag@C**), 9131.1 ± 1684.2 $min^{-1}g^{-1}$ (**Au@C**), 3740.9 ± 313.5 $min^{-1}g^{-1}$ (**Pt@C**), and 11407.4 ± 2260.3 $min^{-1}g^{-1}$ (**Pd@C**) (Table 1). In all instances, the reaction traces remained identical and led to the emergence of a peak at λ_{max} = 302 nm (Fig. 2). Critical to the employment of the cocktail is the necessity for limiting competing side reactions between the individual components (both reagents and products). To demonstrate lack of side reactions, individual reagent and product spectra from 0.39 µmol solutions were plotted. Next, spectral deconvolution (OriginPro 2020, Peak Deconvolution App) was carried out for the reagent components which constitute the bimodal peak, and for the product components which constitute the monomodal peak. The calculated peak centers, areas, and full width at half max were then fed back into the deconvolution software, where it was used to generate the

cumulative peak and compared to the experimental trace from the cocktail (Fig. S4 and S5). Notably, cumulative peak shapes offer a very good fit to experimental spectra. Slight differences in the intensity (reagents experimental shows higher intensity) and spectral shifting (products experimental blue shifts 2 nm) arise from changes in molar absorptivity due to different environmental conditions (single component vs cocktail) and [$NaBH_4$] in solution after reduction of 0.39 µmol of substrate vs 1.56 µmol.[18] Ultimately, the spectral components point to no persistent unexpected products within the timescale measured.

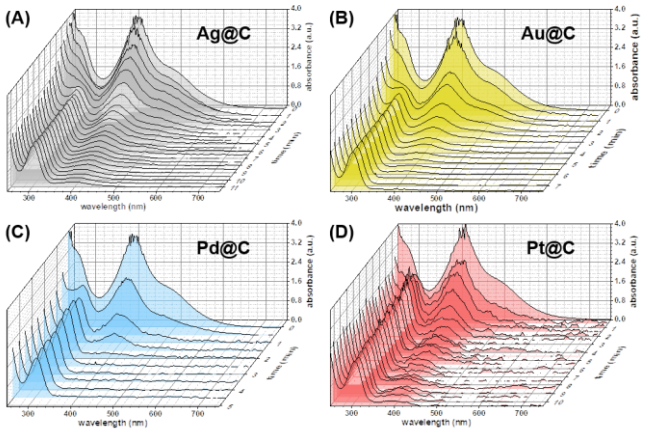

Figure 2. UV-Vis spectra for the catalytic reduction of a nitrophenol cocktail by (A) **Ag@C**, (B) **Au@C**, (C) **Pd@C**, and (D) **Pt@C** in DIW with excess $NaBH_4$.

To expand the scope of azo-substrates, reduction of **AB** was conducted under slightly modified conditions to accomodate solubility (*vide supra*). In this instance, all catalysts showed selectivity towards the partial reduction to hydrazobenzene (**HAB**) instead of the anticipated aniline (Scheme 2). *In situ* monitoring followed the decrease in absorbance at λ_{max} = 322 nm (*trans*-**AB**) with product peaks appearing at λ_{max} = 244 nm and λ_{max} = 288 nm, consistent with **HAB** (Fig. S6 and S7).[19,20] Normalization to %metal content yielded high *K* values across the board: 10808.5 ± 183.7 $min^{-1}g^{-1}$ (**Ag@C**), 24411.8 ± 3173.5 $min^{-1}g^{-1}$ (**Au@C**), 13484.4 ± 728.2 $min^{-1}g^{-1}$ (**Pt@C**), and 12592.6 ± 1762.9 $min^{-1}g^{-1}$ (**Pd@C**) (Table 1). This similarity in selectivity across all four catalysts facilitates the azo reduction comparison.

To compare the predictivity of catalyst performance for the **4NP** screen and the nitrophenol cocktail screen as applied towards azo bond reduction, *K* was normalized across each substrate set and represented as a percentage value for each catalyst. This creates three subsets for visual comparison, i.e. **4NP**, cocktail, and Azo avg, the latter being the average performance across **AB**, and the previously reported **MO** and **MR** reductions (Tables 1 and S2). A graphical representation is depicted in Figure 3. Notably, the inset illustrates the % +/- for over and underrepresentation. Clearly, the **4NP** screen dramatically overestimates the peformance of **Pd@C** and similarly underestimates that of **Pt@C**. By contrast, the cocktail screen yields a tighter grouping, more closely resembling the broader average performance of the catalysts tested. For example, whereas the **4NP** screen immediately discounts both **Ag@C** and **Pt@C** and emphatically promotes only **Pd@C**, the cocktail screen highlights significant performance from **Au@C** and reduced, but notable activity from **Pt@C**.

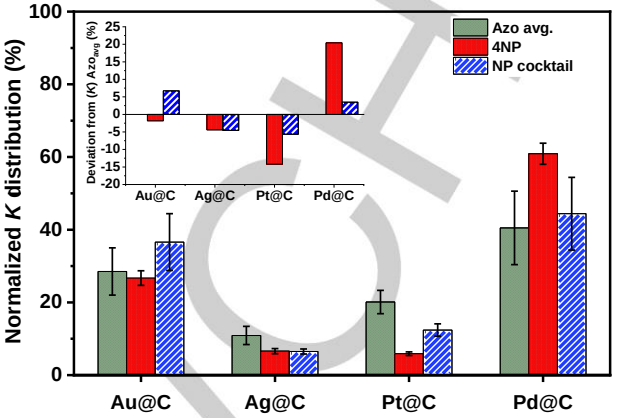

Figure 3. Comparison of normalized *K* values across all catalysts tested for the **4NP** and cocktail screens, compared to the average for azo substrates **AB**, **MO** and **MR** (see Tables 1 and S2).

Extending the reaction screening to the reduction of methylene blue (**MB**)[21] to leucomethylene blue (**LMB**) reveals a limitation for the predictability of the cocktail screening (Fig. 3). In situ monitoring of the decreased in absorbance at λ_{max} = 663 nm revealed very high k_{app} for both **Pt@C** and **Pd@C** (2.75 min^{-1}, and 4.75 min^{-1} respectively) commensurate with rapid decoloration.[22] Notably, the solutions were very turbid due to the rapid and continuous evolution of H_2 from $NaBH_4$ hydrolysis (Scheme 1). Conversely, **Ag@C** and **Au@C** yielded lower k_{app} values (0.16 min^{-1} and 0.19 min^{-1} respectively), and most importantly, maintained an equilibrium between **MB** and **LMB**, with a gradual shift towards **MB** as the $NaBH_4$ concentration decreased (Fig. S9 and S10). Solution turbidity in both cases was substantially lower, which allows the reversal of the reduction to occur by interaction with dissolved O_2; a common phenomenon with **MB** reduction.[23,24] We postulate that the rapid generation of H_2 by **Pt@C** and **Pd@C** serves to purge O_2 from the system, circumventing the redox equilibrium. In this instance, this secondary process interferes with the accurate assesment of reduction rate and provides poor correlation to the cocktail screening protocol.

Figure 3. Catalytic reduction of methylene blue (**MB**) by metal nanoparticles in DIW with excess $NaBH_4$. (*inset*) Picture of a solution denoting associated color changes.

Table 1. summary of mass normalized reaction rates (*K*)

Catalyst	[a]MO	[a]MR	AB	[a]4NP	cocktail	cocktail	cocktail
	K ($min^{-1}g^{-1}$)	K ($min^{-1}g^{-1}$)	K ($min^{-1}g^{-1}$)	K ($min^{-1}g^{-1}$)	K^1 ($min^{-1}g^{-1}$)	K^2 ($min^{-1}g^{-1}$)	K_{avg} ($min^{-1}g^{-1}$)
Ag@C	2311.9 ± 226.6	2285.4 ± 498.8	10808.5 ± 183.7	3608.06 ± 376.2	1361.7 ± 23.1	1957.5 ± 33.3	1659.6 ± 40.5
Au@C	7282.6 ± 860.1	6628.8 ± 122.9	24411.8 ± 3173.5	14648.86 ± 1011.4	8394.7 ± 1091.3	9867.5 ± 1282.8	9131.1 ± 1684.2
Pt@C	4718.1 ± 144.9	6339.6 ± 483.4	13484.4 ± 728.2	3219.08 ± 233.9	2050.4 ± 110.7	5431.7 ± 293.3	3740.9 ± 313.5
Pd@C	27147.8 ± 1974.9	8363.7 ± 212.9	12592.6 ± 1762.9	33451.73 ± 1244.8	10962.9 ± 1534.8	11851.9 ± 1658.3	11407.4 ± 2260.3

[a] values reported in ref. 15

In summary we have shown additional reactivity for our previously reported catalyst set; namely reduction of methylene blue which is enhanced by solution turbidity via complementary H_2 generation from $NaBH_4$ hydrolysis, and selective azobenzene semihydrogenation. Most importantly, we have endeavored to develop a cocktail screening methodology which overcomes the catalyst specificity of the **4NP** reduction reaction, with the hope of improving catalyst down-selection. The example presented herein is a proof of concept that multiple nitrophenols can be reduced in concert without deleterious side reactions, and their overall rate similarly logged by facile UV-Vis measurement and kinetic interpretation. The result thereof appears to yield an improved understanding of relative catalyst performance when compared, inherently, to a broader nitrophenol substrate scope, and to azo bonds. Our ongoing focus is on the discovery of improved reagent cocktails, and an expansion of the comparative library of reducible moieties beyond azo functional groups. The ultimate goal is the development of a "tool box" of screening protocols for accurate catalyst down-selection.

Acknowledgements

This work was supported by the Departments of Chemistry and Physics, College of Science, and the FCI at the University of Central Florida. A. P. Sattelberger, UCF, is thanked for helpful discussions.

Keywords: nitrophenol • heterogeneous catalysis • nanoparticles • catalytic hydrogenation • catalyst screening

[1] (a) S. Yi, W.-Q. Zhuang, B. Wu, S. Tiong-Lee, J-H. Tay, *Environ. Sci. Technol.* **2006**, *40*, 2396-2401; (b) M. R. H. Podeh, S. K. Bhattacharya, M. Qu, *Water Res.* **1995**, *29*, 391-399; (c) J. Xia, G. He, L. Zhang, X. Sun, X. Wang, *Appl. Catal., B* **2016**, *180*, 408-415; (d) S. Yu, J. Hu, J. Wang, *J. Hazard. Mater.* **2010**, *177*, 1061-1067.

[2] (a) K.-S. Ju, R. E. Parales, *Microbiol. Mol. Biol. Rev.* **2010**, *74*, 250-272; (b) H. Zhao, C.-H. Kong, *Chem. Eng. J.* **2018**, *339*, 424-431; (c) M. Sun, D. D. Reible, G. V. Lowry, K. B. Gregory, *Environ. Sci. Technol.* **2012**, *46*, 6174-6181.

[3] (a) R. S. Downing, P. J. Kunkeler, H. van Bekkum, *Catal. Today* **1997**, *37*, 121-136; (b) G. Wegener, M. Brandt, L. Duda, J. Hofmann, B. Klesczewski, D. Koch, R.-J. Kumpf, H. Orzesek, H.-G. Pirkl, C. Six, C. Steinlein, M. Weisbeck, *Appl. Catal., A* **2001**, *221*, 303-335; (c) K. Nomura, *J. Mol. Catal. A: Chem.* **1998**, *130*, 1-28; (d) M. Espinosa Bosch, A. J. Ruiz Sánchez, F. Sánchez Rojas, C. Bosh Ojeda, *J. Pharm. Biomed. Anal.* **2006**, *42*, 291-321.

[4] Z. Xiong, H. Zhang, W. Zhang, B. Lai, G. Yao, *Chem. Eng. J.* **2019**, *359*, 13-31.

[5] S. Gu, S. Wunder, Y. Lu, M. Ballauf, R. Fenger, K. Rademann, B. Jaquet, A. Zaccone, *J. Phys. Chem. C.* **2014**, *118*, 18618-18625.

[6] M. Nasrollahzadeh, Z. Nezafat, M. G. Gorab, M. Sajjadi, *Mol. Catal.* **2020**, *484*, 110758.

[7] (a) T. Aditya, A. Pal, T. Pal, *Chem. Commun*. **2015**, *51*, 9410-9431; (b) N. Pradhan, A. Pal, T. Pal, *Colloids surf., A*., **2002**, *196*, 247-257 (c) J. Strachan, C. Barnett, A. F. Masters, T. Maschmeyer, *ACS Catal.* **2020**, *10*, 5516-5521.

[8] P. Zhao, X. Feng, D. Huang, G. Yang, D. Astruc, *Coord. Chem. Rev.* **2015**, *287*, 114-136.

[9] P. Hervés, M. Pérez-Lorenzo, L. M. Liz-Marzán, J. Dzubiella, Y. Lu, M. Ballauff, *Chem. Soc. Rev.* **2012**, *41*, 5577-5587.

[10] N. C. Antonels, R. Meijboom, *Langmuir* **2013**, *29*, 13433-13442.

[11] S. Wunder, Y. Lu, M. Albrecht, M. Ballauf, *ACS Catal.* **2011**, *1*, 908-916.

[12] S. Wunder, F. Polzer, Y. Lu, Y. Mei, M. Ballauf, *J. Phys. Chem. C* **2010**, *114*, 8814-8820.

[13] R. Grzeschik, D. Schäfer, T. Holtum, S. Küpper, A. Hoffmann, S. Schlücker, *J. Phys. Chem. C.* **2020**, *124*, 2939-2944.

[14] (a) N. E. Larm, N. Bhawawet, J. A. Thon, G. A. Baker, *New. J. Chem.,* **2019**, *43*, 17932-17936; (b) U. I. Kramm, R. Marschall, M. Rose, *ChemCatChem*, **2019**, *11*, 2563-2574.

[15] L. R. Shultz, L. Hu, K. Preradovic, M. J. Beazley, X. Feng, T. Jurca, *ChemCatChem*, **2019**, *11*, 2590-2595.

[16] L. R. Shultz, B. McCullough, W. J. Newsome, H. Ali, T. E. Shaw, K. O. Davis, F. J. Uribe-Romo, M. Baudelet, T. Jurca, *Molecules*, **2020**, *25*, 89.

[17] (a) H. I. Schlesinger, H. C. Brown, A. E. Finholt, J. R. Gilbreath, H. R. Hoekstra, E. K. Hyde, *J. Am. Chem. Soc.* **1953**, *75*, 215-219; (b) R. Retnamma, A. Q. Novais, C. M. Rangel, *Int. J. Hydrogen Energ.* **2011**, *36*, 9772-9790.

[18] M. F. Vitha, *Spectroscopy Principles and Instrumentation*, 2019, Wiley, NJ, USA

[19] C. Tosi, *Spectrochimica Acta*, **1966**, *22*, 399-402.

[20] (a) Y. Shiraishi, M. Katayama, M. Hashimoto, T. Hirai, *Chem. Commun.* **2018**, *54*, 452-455; (b) H. Abdullah, D.-H. Kuo, N. S. Gultom, *Catal. Sci. Technol.* **2019**, *9*, 2651-2663.

[21] (a) S. Du, Z. Liao, Z. Qin, F. Zuo, Z. Li, *Catal. Commun.* **2015**, *72*, 86-90; (b) S. Hemmati, L. Mehrazin, H. Ghorban, S. H. Garakani, T. H. Mobaraki, P. Mohammadi, H. Veisi, *RSC Adv.* **2018**, *8*, 21020-21028; (c) N. R. Jana, T. K. Sau, T. Pal, J. *Phys. Chem. B.* **1999**, *103*, 115-121.

[22] C. Corredor, M. D. Borysiak, J. Wolfer, P. Westerhoff, J. D. Posner, *Environ. Sci. Technol.* **2015**, *49*, 3611-3618.

[23] X. Bi, H. Ma, P. Westerhoff, *Environ. Sci. Technol.* **2018**, *52*, 13289-13297.

[24] A similar O_2-mediated reversible reaction between nitrosophenol and nitrophenol is proposed to occur during the induction period prior to rapid reduction: (a) J. Strachan, C. Barnett, A. F. Masters, T. Maschmeyer, *ACS Catal.* **2020**, *10*, 5516-5521; (b) E. Menumerov, R. A. Hughes, S. Neretina, Nano Lett. 2016, 16, 7791-7797; (c) R. D. Neal, Y. Inoue, R. A. Hughes, S. Neretina, J. Phys. Chem. C. 2019, 123, 12894-12901.

Entry for the Table of Contents

Catalytic reduction of 4-nitrophenol is the benchmark model for testing catalytic activity of nanoparticles. A single molecule probe is however prone to disparate selectivity leading to false rankings for catalyst down-selection. We report a facile multi-nitrophenol cocktail screening method. When tested with noble metal nanoparticles, the cocktail approach provides improved ranking of relative catalyst activity when compared to reduction of azo bonds.